Multiple-return laser radar for three-dimensional imaging through obscurations

Bradley W. Schilling, Dallas N. Barr, Glen C. Templeton, Lawrence J. Mizerka, and C. Ward Trussell

A compact imaging laser radar was constructed and tested to investigate phenomenological issues in targeting, especially cases involving imaging through obscurations such as foliage and camouflage netting. The laser radar employs a Nd:YAG microchip laser that operates at a wavelength of 1.06 μm and produces pulses of 1.2-ns duration at a 3-kHz rate. The detector is a commercial indium gallium arsenide avalanche photodiode. A single computer controls the scanning mirrors and performs the digitization of the returning signal at 2 giga samples/s. A detailed description of the laser radar is presented as well as results from field experiments that examined its range accuracy capability and its ability to image a target through camouflage. Results of data collected from deciduous tree lines are also discussed to characterize the presence and quantity of multiple returns. © 2002 Optical Society of America

OCIS codes: 280.0280, 280.3640, 110.0110, 110.6880.

1. Introduction

Three-dimensional (3-D) imaging for remote sensing applications is one of the most active and productive areas of electro-optical research and development, in part because the problems are challenging and interesting. Much of the early research in this field involved atmospheric aerosol measurement by CO_2 laser-based systems,[1–5] and this research continues today. More recently, advances in solid-state lasers such as Nd:YAG have made it possible to accomplish atmospheric remote sensing at near-infrared wavelengths.[6,7] Requirements for military, commercial, and space-based applications such as obstacle detection, target identification, terrain mapping, and navigational guidance are also being addressed by various types of laser radar system currently under development.[8–10] One particularly challenging problem is the military requirement to identify targets that are partially obscured by man-made or natural obscurants, such as camouflage netting, foliage, smoke, or fog. Similar commercial and law enforcement needs include terrain mapping below a foliage canopy, surveillance through foliage, and agricultural monitoring. Recent advances in laser- and computer-related systems have made it possible for us to develop a direct detection laser radar system with enhanced capability to identify targets behind such obscurations. A key difference between our system and other laser radars stems from the capability to digitize and store the entire return pulse (for a software-selectable range gate of interest.) We briefly describe the basic principle of operation and system architecture of the laser radar system. Field trial results demonstrate the system capabilities, with emphasis on 3-D imaging in the presence of obscurations such as foliage and camouflage netting.

2. Principle of Operation

Our laser radar is based on standard direct detection laser-ranging principles. For a single ranging operation a short pulse of laser radiation is generated by the transmitter, formed by beam shaping optics, and directed toward the target or area of interest. The laser radiation travels through the atmosphere, is scattered by whatever it hits, and a small portion of the laser radiation is reflected directly back to the transceiver. The returned optical energy is collected and focused by receiving optics onto a photodetector, which generates a voltage proportional to the optical

B. W. Schilling (bradley.schilling@nvl.army.mil), D. N. Barr, G. C. Templeton, L. J. Mizerka, and C. W. Trussell are with the U. S. Army Communications and Electronics Command Research, Development and Engineering Center, Night Vision and Electronic Sensors Directorate, 10221 Burbeck Road, Suite 430, Fort Belvoir, Virginia 22060.

Received 13 November 2001; revised manuscript received 1 February 2002.

0003-6935/02/152791-09$15.00/0

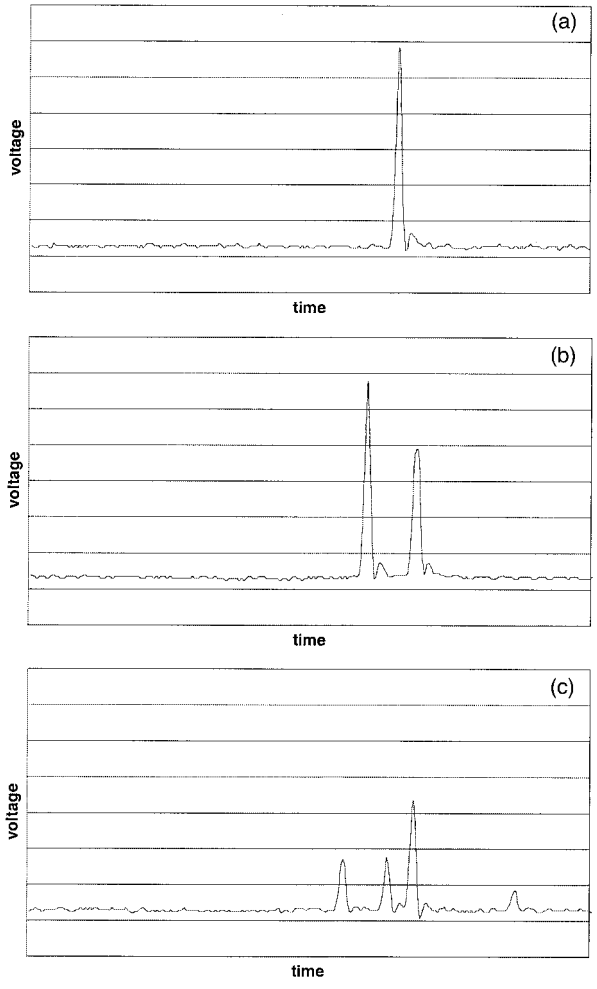

Fig. 1. Plots showing typical return signals from different types of target: (a) single return, (b) double return, (c) multiple return.

power received. The range to the target is determined by measurement of the round-trip time necessary for the laser pulse to travel to the target and back to the receiver, which is collocated with the transmitter at the transceiver head. For an imaging laser radar, such as the one presented here, the ranging process is repeated for each pixel in the scene of interest when the laser is scanned in a raster fashion.

The temporal characteristics of the return signal are dependent on the object or objects that intercept the beam as it propagates away from the transmitter.[11] For example, an extended, flat target that intercepts the entire beam results in a single-pulse return on the photodetector, as shown in Fig. 1(a). However, if the laser beam is only partially intercepted by an object, some portion of the outgoing energy is scattered whereas the remaining energy continues to propagate forward. If a second object lies in the path of the laser beam, behind the first object, some or all of the remaining energy will be scattered. The second return occurs from a greater distance, corresponding to a later time. As a result, the return signal will contain two pulses, as shown in Fig. 1(b). The partial scattering case can easily manifest itself as many return pulses for certain obscurations, such as foliage or camouflage netting. A representative laser radar return signal from heavy foliage consisting of trees and branches is shown in Fig. 1(c). Multiple returns such as that shown in Fig. 1(c) are common, especially in military situations, and most tactical laser range finders provide a multiple-target indication. Typically the tactical laser range finder provides the range measurement corresponding to either the first return or the final return received during a lasing operation, which is referred to as first-pulse–last-pulse logic.[12]

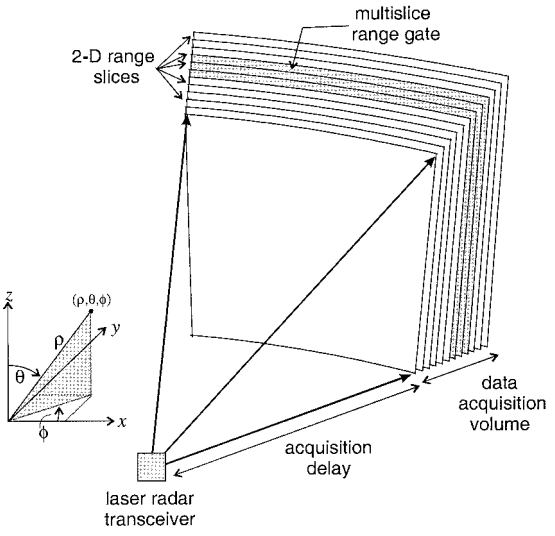

Fig. 2. Laser radar data can be displayed as a 2-D range-gated image.

It is clear from Fig. 1 that a great deal of target information is contained in the entire return signal. This is especially true for targets obscured by foliage, camouflage netting, smoke, or other obscurations. Traditionally, this information has been discarded by incorporation of either first-pulse or last-pulse logic for range finding and laser radars.[12] Our laser radar system, on the other hand, digitizes and stores the entire return pulse (for a software-selectable range gate of interest.) This factor is key to enhance targeting capabilities through obscurations and is what makes our system different from other laser radars.

Figure 2 illustrates the effect of digitizing and storing the return signal for a range gate of interest. The laser radar data set consists of a 3-D array of 8-bit intensity values, represented in Fig. 2, as a series of two-dimensional (2-D) range slices. The data volume is determined in θ and ϕ by the scanning parameters and in ρ by the digitization length of the avalanche photodiode (APD) signal. The temporal separation of each 2-D range slice is determined by the digitization frequency (f_d) and corresponds to the spatial range slice depth of

$$r = \frac{c}{2f_d}, \tag{1}$$

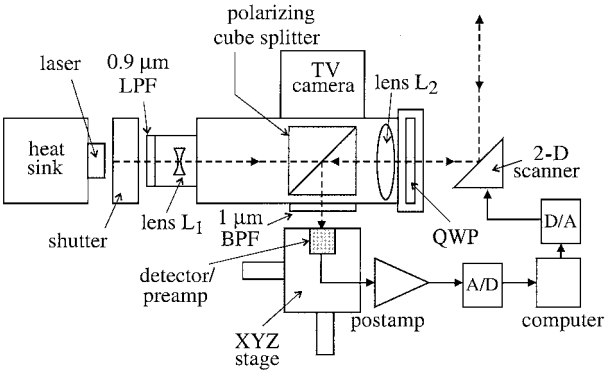

Fig. 3. Transceiver layout. LPF, long-pass filter; QWP, quarter-wave plate; BPF, bandpass filter; D/A, digital-to-analog; A/D, analog-to-digital.

where c is the velocity of light. Laser radar data can be displayed in a number of ways, from a 2-D intensity image showing a single range slice to a full 3-D rendering of the entire volume of data. Somewhere between these two representations is the display of multiple range bins to show a specific range-gated volume. Examples of each of these display techniques are given in Section 4.

3. Laser Radar Architecture

The laser radar transceiver architecture is based on standard direct detection laser ranging. A microchip laser generates bursts of high peak power, short-pulse laser radiation that are scanned over the area of interest. Scattered radiation is collected by the receiver, which has a common aperture with the transmitter at the transceiver head. The transmitted beam and received signals are separated by polarization. The laser radar return signals are digitized and stored, resulting in a 3-D array of data representing the entire volume of interest. The optical layout, consisting of a collection of commercially available components, is shown in Fig. 3.

The laser source, a Nd:YAG microchip laser (Litton Airtron Synoptics), has an operating wavelength of 1.06 μm. Individual pulses produced by the microchip laser have an energy of approximately 6.0 μJ, a pulse width of 1.2 ns, and are emitted at a rate of 3.0 kHz. These laser parameters result in a laser hazard classification of 3b, in accordance with American National Standards Institute Z136.1. To reduce the nominal ocular hazard distance, a computer-controlled shutter allows only laser radiation to be emitted when the scanners are active. Also, for safety reasons, an optical long-wave pass filter is positioned at the entry aperture of the telescope to block radiation emitted from the diode laser pump, an integral component of the microchip laser package. A diverging lens L_1 serves as the telescope secondary optic, which in conjunction with the primary lens L_2 offers a system beam divergence of approximately 100 μrad. As shown in Fig. 3, the laser radiation passes through a polarization beam splitter between the secondary and primary lenses of the beam expander. Immediately after lens L_2, the linearly polarized radiation is converted to circular polarization by the 35-mm-diameter quarter-wave plate, the last element of the optical path before the scanners, and the limiting aperture for the sensor. Two galvanometer scanning mirrors direct the laser radiation to the area of interest, scanning the scene in a raster fashion.

Reflected radiation is collected by the scanning mirrors, focused by lens L_2 and directed by the polarization beam splitter to an InGaAs APD and preamplifier module (Fujitsu Model FRM5W231DR). The APD preamplifier has a 2.5-GHz bandwidth and a 30-μm-diameter active area. Taking into account the focal length of the lens L_2, which is nominally 100 mm, the field of view of the receiver is 300 μrad. A MiniCircuits Model 500 LN postamplifier with a bandwidth of 500 MHz further amplifies the output of the detector preamplifier, resulting in the final receiver signal that is sent to the computer.

As stated above, our system's enhanced capability to detect objects behind or through obscurations stems from the short laser pulse coupled with high-speed digital sampling and storage of the entire return signal over a time period of interest. The analog-to-digital (A/D) board for digitizing the return signal is an Acqiris DP210, 2-giga sample/s data-acquisition board. In the reported configuration, a computer-controlled digital-to-analog board sends the (θ, ϕ) drive voltages to the galvanometric scanning mirrors, for positioning, and enables the A/D acquisition board. The laser is free running, so the next outgoing pulse triggers the acquisition board. After a software-selectable delay, the acquisition board begins to digitize the photodetector signal. The number of samples acquired is predetermined and software selectable. After the acquisition is completed, the computer sends the coordinates (voltages) for the next scan point, repeating the process in a raster pattern for the entire data set. There are two basic modes of operation, a single-shot acquisition, as described, and a four-shot average mode. In the averaging mode, the scanners dwell at each scan position for four complete digitization operations of the APD signal, within the desired range gate. The A/D board stores each acquisition in on-board memory, conducts an arithmetic average on the fly, and transfers the resultant averaged signal trace to the PC. A $256 \times 256 \times 256$ single-shot scan takes approximately 40 s to complete in the current configuration, and a four-shot averaged acquisition requires approximately 90 s.

4. Breadboard Laser Radar Results

A. General Display and Processing Characteristics

As described in Section 2, the laser radar system digitizes and stores the entire detected laser pulse for each position in the scan, allowing for enhanced imaging capabilities through obscurations. The product of a laser radar acquisition operation is a 3-D array of 8-bit intensity values that is $256 \times 256 \times 256$

Fig. 4. Photograph of truck used in laser radar data collection.

in size. Along with minimal header information, each data set requires approximately 16.5 Mbytes of computer storage, uncompressed.

To describe common digital processing algorithms and display techniques involved in laser radar data, we present an example data set taken of a white crew-cab pickup truck, at a range of 55 m, shown photographically in Fig. 4. Horizontal and vertical scan voltages corresponding to a full-angle scan of 97.0 mrad and a scan step size of 379 μrad were used for this data acquisition. Note that, with a beam divergence of approximately 100 μrad, our step size is approximately four times the beam size. Figures 5 and 6 demonstrate two different types of processing and display of the laser radar data of the pickup truck, the first based on the intensity of the return signal and the second based on range information.

The initial phase of digital processing involves range gating and peak detection. The images shown in Figs. 5 and 6 are a 2-D representation of a limited set of range slices encompassing the target, or area, of interest (see Fig. 2). For example, information contained in a 61-bin range gate, from approximately 54 to 59 m, is displayed in Figs. 5 and 6. Subsequent to selecting a range gate, we applied a peak detect algorithm along the longitudinal dimension of the laser radar data set, thus reducing the 3-D volume of information into a 2-D image. That is, for each (θ, ϕ) pixel in Fig. 5, the intensity of the ρ pixel having the maximum return, within the range gate of interest, is displayed. Figure 6, on the other hand, is a range

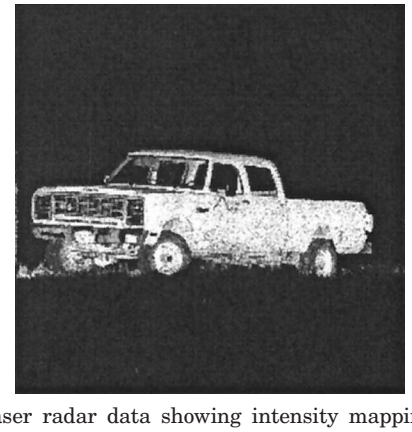

Fig. 5. Laser radar data showing intensity mapping of truck. The range gate is approximately 54–59 m.

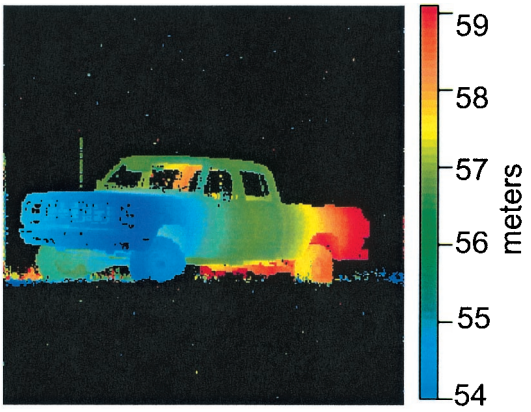

Fig. 6. Laser radar data showing range mapping of truck. The range gate is approximately 54–59 m.

representation of the same information. At each (θ, ϕ) location in Fig. 6, a color pixel is displayed indicating the range to the ρ pixel having the maximum return, again within the preselected range gate. In Fig. 6, blue is used to show the shortest range, varying shades of green and yellow represent intermediate ranges, and red indicates the farthest range in this image.

A combination of range gating and peak detection reduces the laser radar information from a 3-D volume to a 2-D image. A second phase of digital processing is then applied to the laser radar images, primarily for display purposes. An intensity map, such as that shown in Fig. 5, undergoes a digital normalization process. The largest returns are assigned a gray-scale value of 255 (white), low returns are assigned a value near zero (black), and a linear distribution is applied to intermediate values. Areas containing no strong return signal (such as the sky above the truck) are normalized to a gray-scale level near black. This is not the case, however, for the range-mapped image shown in Fig. 6. Because the color assigned to the image pixel is based entirely on the range information and not the signal strength, each pixel in the image is assigned a color corresponding to the range of the peak return at that (θ, ϕ) point. Therefore threshold processing is also required to generate an image such as Fig. 6. Applying a digital threshold allows us to display pixels containing low signals as black; while color range mapping is used only for stronger returns.

B. Range Accuracy

To investigate the relative range accuracy of our laser radar, a data collection was taken of a 4 ft × 8 ft (1.22 m × 2.44 m) target board with an adjustable 1-ft- (0.305-m-) square central piston. The plywood target board was painted gray with a 20% reflectivity at 1.06 μm. Horizontal and vertical scan voltages corresponding to a full-angle scan of 37.3 mrad and a scan step size of 146 μrad were used for this data acquisition. Note that, with a beam divergence of approximately 100 μrad, our scanning step size is approximately 1.5 times the beam size. Figures 7

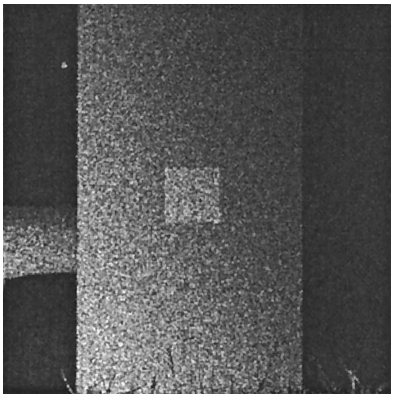

Fig. 7. Single range slice of the target board at 57.3 m.

and 8 show intensity and range results with the central piston positioned 1.5 in. (3.81 cm) in front of the target board. Figure 7 shows a single range slice at 57.3 m in which the central piston is clearly discernable from the target board. To digitally extract a single range slice (a 2-D image of constant range) from the 3-D volume of data, the 2-D (θ, ϕ) array of intensity values is simply extracted from the 3-D array for a given constant ρ. The 2-D image is then normalized to enhance the dynamic range and contrast for display purposes. A narrow range gate consisting of four range bins is displayed in Fig. 8, in which four colors representing range bins separated by 0.075 m are distinguishable across the target board. Again, the piston of differing range is apparent in the range-mapped image. It is clear from both Figs. 7 and 8 that the target board is leaning slightly away from normal to the laser radar scanning pattern in that the lower left corner of the board is closest, whereas the upper right corner is farthest from the transceiver. It is interesting that, for any given pixel, a range accuracy of approximately 3 in. (8 cm) is achievable based on the sampling rate, in accordance with Eq. (1). However, it is possible to distinguish range differences of less than 3 in. for an area target, such as the target board and piston. As the laser radar scans an area situated between two absolute range bins, the statistical distribution of measured ranges for that area is related to the actual range. If the actual range is closer to the range bin corresponding to the yellow pixels, for example, there will be more yellow pixels in the area than some other color, say green. It should be possible to obtain a more accurate range estimation of surfaces that lie between range bins by a statistical analysis over the area of interest. Similarly, for the human observer, the eyes have a tendency to spatially average the pixel data over an area. In this manner, we are able to distinguish areas containing range differences of less than the absolute range capability of the laser radar for a single pixel. Similarly, even though only four range bins are represented in the returns from the entire target board shown in Fig. 8, the observer can (arguably) distinguish nearly twice as many separate ranges in the color representation. For example, the observer may claim to distinguish a yellow region, an orange region, and a yellowish orange region. A data collection was conducted with the piston positioned 1.0 in. (2.54 cm) in front of the target board, but the results (not shown here) indicate that the piston is indistinguishable from the target board in that case. By incorporating slightly more advanced digital processing, such as deconvolution, which has been applied to long-pulse laser radar signals,[13,14] our overall depth accuracy can be improved.

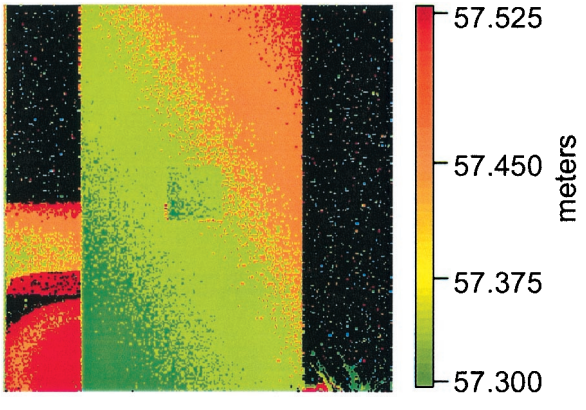

Fig. 8. Multiple-slice range map of the target board.

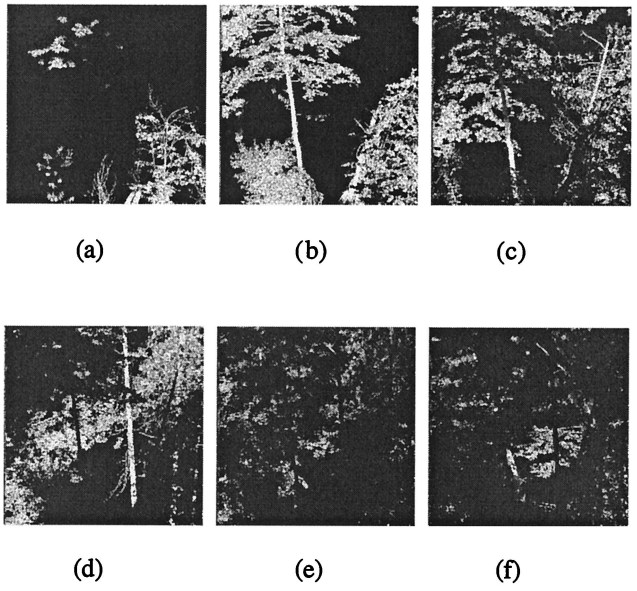

Fig. 9. Range-gated intensity images extracted from a single laser radar acquisition. Ranges in meters are (a) 56.7–59.0, (b) 59.0–61.2, (c) 61.2–63.5, (d) 63.5–65.7, (e) 65.7–67.9, (f) 67.9–70.2.

C. Investigation of Multiple-Pulse Data

The laser radar imagery of Figs. 5–8 is representative of typical data that could have been generated with a first-pulse–last-pulse logic-based direct detection system. To demonstrate the enhanced capability gained from keeping multiple-return information, we conducted a laser radar acquisition of an area with dense foliage. Figure 9 shows a series of six

Table 1. Return Pulse Statistics for the Data Set Shown in Fig. 9

Number of Signal Pulses in Laser Return	Number of Occurrences
No return	190
Single	23,246
Double	30,998
Three	7575
Four	871
Five	63
Six	2

range-gated intensity images extracted from that data set. Each image represents intensity information from a 30-bin (approximately 2.2 m) range gate. Digital processing is as described above for Fig. 5. The first range-gated intensity image, Fig. 9(a), corresponds to ranges from 56.7 to 59.0 m. Each subsequent image displays the next 2.2 m of foliage. The six-image set therefore spans a total of approximately 13.2 m.

To quantify the advantage to 3-D imaging gained through fully incorporating multiple-pulse information, we consider the data set of Fig. 9 in greater detail. To acquire valid statistics of multiple-return signals, a small, noisy portion of the data is ignored. The leftmost columns of Fig. 9 contain excess noise, presumably from the scanning mirrors, so the first ten columns are zeroed out prior to pixel counting procedures. Working with this $256 \times 246 \times 256$ sized data set, we count the number of signal pulses present in the entire 3-D volume, where a signal pulse is defined by a threshold-to-noise figure of 6.2, which for our system corresponds to a false-alarm rate of 1.3 Hz.[12] There are 111,778 signal pulses present in the 3-D volume, compared with a possible 62,976 (256×246) if single-pulse logic is employed, indicating that we are able to acquire nearly 1.8 times more information. To determine how that additional information manifests itself, we constructed a histogram of the number of signal pulses present for each laser-ranging operation. These data are presented in Table 1. We can see that 8511 laser-ranging operations, or 13.5%, resulted in three or more laser returns.

It is apparent that important information is present in the interior volume of laser radar returns. To investigate the impact this information has on 3-D image creation, consider a data set equivalent to Fig. 9(f), but recorded by a first-pulse detection system. We can extract this first-pulse data set from our data by digitally eliminating all returns that are received at a time later than the initial pulse for each (θ, ϕ) position. We then impose, on the first-pulse processed data set, the same range gate as in Fig. 9(f). Counting the number of signal pixels in the processed and gated data set tells us the number of returns between 67.9 and 70.2 that are the result of a first-pulse return. That value is 2938 pixels. There are 7185 signal pixels in Fig. 9(f), showing that 4247 (more than half) of the signal pixels in that range gate are the result of a multiple-pulse return. For 3-D imaging in heavy foliage, it is apparent that use of multiple-pulse data can have a significant impact.

Fig. 10. Photograph of camouflage net and white truck.

D. Laser Radar Imaging through Obscurations

The primary advantage of our whole-return detection scheme is an enhanced capability to accomplish 3-D imaging through partial obscurations, such as foliage or camouflage netting. We demonstrate this capability with a practical example. Figure 10 shows a photograph of the white crew-cab pickup truck behind heavy camouflage netting, whereas Figs. 11 and 12 show the corresponding gated range data from the laser radar. The truck is positioned broadside to the transceiver at a range of approximately 57 m. Two camouflage nets are positioned between the transceiver and the truck at ranges of approximately 54 and 55 m. Horizontal and vertical scan voltages corresponding to a full-angle scan of 111.9 mrad and a scan step size of 437 μrad were used for this data acquisition. As we have shown for previous data sets, Fig. 11 is a range-gated intensity map of the vehicle and Fig. 12 is a gated range mapping of the same target. The displayed range gate contains 20 range slices spanning the ranges from 57.6 to 59.8 m. For comparison purposes, we show the identical targeting situation, but without the camouflage netting present, in Figs. 13 and 14. Conducting a similar pixel counting technique as prescribed above, we find that the gated image of the truck without any obscurations contains 9799 signal pixels, whereas Fig. 12 contains 3132 returns. We conclude therefore that

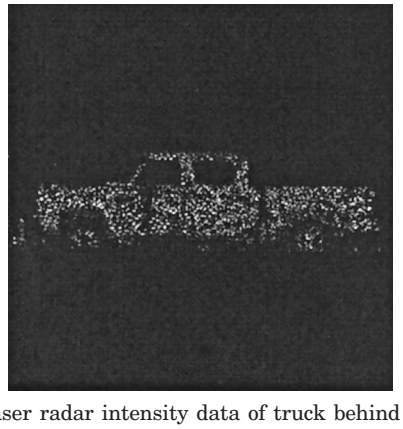

Fig. 11. Laser radar intensity data of truck behind heavy camouflage netting.

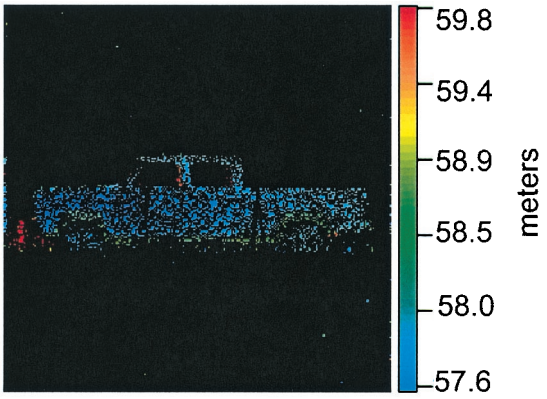

Fig. 12. Laser radar range data of truck behind heavy camouflage netting.

we are able to detect approximately 32% of the target information through a double camouflage net.

Advanced techniques for target identification through dense foliage involve combining several laser radar data sets of the same general area, but acquired from different transceiver positions.[15] For this case, as the look angle to the target changes, different portions of the target become visible to the sensor through the foliage. With each data acquisition, a little more of the target is pieced together until a positive identification is possible. According to Zheng *et al.,* target identification is possible with 200 pixels on target, provided that the data have a high signal-to-noise ratio and adequate range accuracy (15 cm or better).[16] Interestingly, a similar situation arises (without moving the transceiver), under windy conditions, because of the constant movement of the foliage.

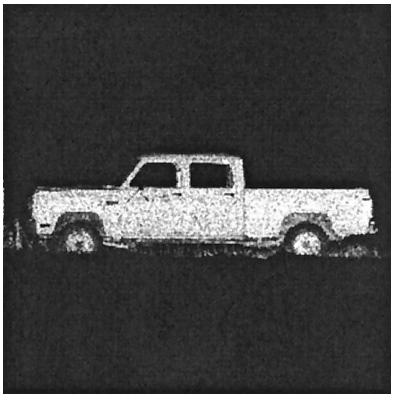

Fig. 13. Laser radar intensity data of truck without camouflage netting.

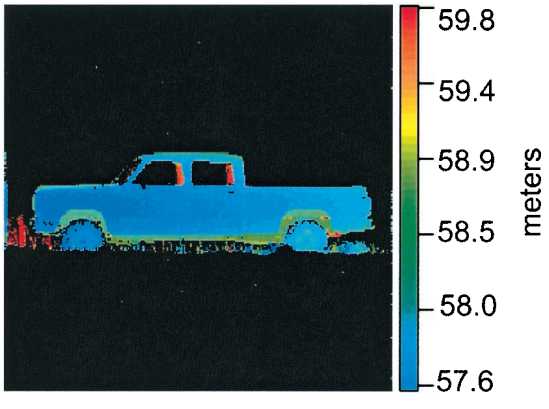

Fig. 14. Laser radar range data of truck without camouflage netting.

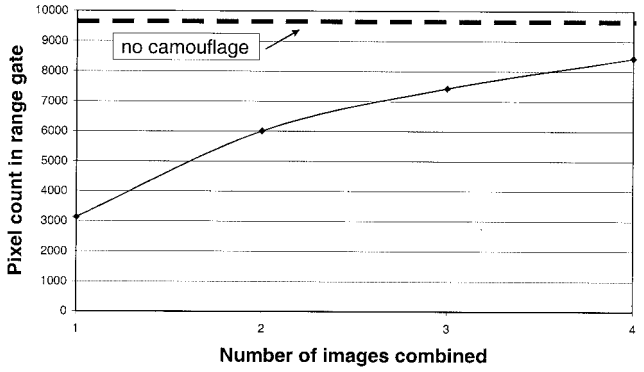

Fig. 15. Results of pixel counting in a selected range gate for the combined data.

To investigate this concept we conducted several data acquisitions having the same rudimentary qualities as the multiple look-angle case. We repeated the data collection of Figs. 11 and 12 but moved the camouflage netting slightly between data acquisitions. We then combined two of these data sets by first range gating to eliminate the camouflage netting from the data set. Second, the peak detection algorithm is invoked on each gated image. Finally, the images are compared on a pixel-by-pixel basis. At each (θ, ϕ) position, the maximum intensity value of the two images is kept and inserted into the final (processed) image. Thus the important target pixels from each acquisition are pieced together into a single data set. This processing is similar to ORing, except the intensity value is maintained. Mathematically, this can be described by the following:

$$I(\theta, \phi) = \max[I_1(\theta, \phi), I_2(\theta, \phi)], \qquad (2)$$

where $I(\theta, \phi)$ is the intensity of the processed image at position (θ, ϕ), $I_1(\theta, \phi)$ is the corresponding intensity value for the first data set, and $I_2(\theta, \phi)$ is the intensity of the pixel in the second data set. We evaluate the effectiveness of piecing together the target in this manner by counting the total signal pixels in the range gate of the truck after multiple implementations of Eq. (2). We make a comparison with the number of returns from the unobscured vehicle (Figs. 13 and 14). A plot of four such operations is shown in the graph of Fig. 15. Figure 15 shows that, when two images are combined in this fashion, nearly twice as many laser returns are detected from the target, thus increasing the percentage from approximately 32% to 61% of the returns from the unobscured vehicle. Combining data from a third look increased the overall number of pixels to 76%, and a fourth

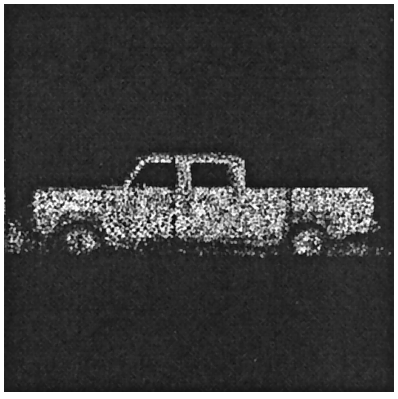

Fig. 16. Laser radar intensity data of truck behind heavy camouflage netting after four images are combined digitally.

combination resulted in 86% of the possible target pixels being received. Intensity and range mappings of four data sets, individually acquired through double camouflage netting and subsequently processed in accordance with Eq. (2) to form one image, are shown in Figs. 16 and 17.

5. Conclusions

We have presented a direct detection-based imaging laser radar system designed to investigate 3-D imaging through obscurations such as foliage and camouflage netting. The operating wavelength of the laser radar is 1.06 μm, employing a Nd:YAG microchip laser and an indium gallium arsenide APD. The key technology enabler to image through obscurations is a detection scheme that includes a fast A/D operation, digitizing and storing the entire return pulse (within selectable limits) for each ranging operation. When imaging through obscurations, such as foliage, target information manifests itself in multiple laser returns. We incorporated multiple-return information into our 3-D images rather than discarding it, as is the case with first-pulse–last-pulse logic-based systems. In a case study of 3-D foliage data, analysis shows that 63% of the ranging operations contained two or more return pulses, and 13.5% contained three or more returns. We have also offered a brief analysis of sophisticated 3-D targeting techniques that piece together information from multiple data collections. In our case, laser radar data were collected of a target approximately 70% obscured by heavy camouflage netting. Between data acquisitions, the camouflage was moved slightly or allowed to blow in the wind. By combining target information from different acquisitions, we were able to image 86% of the possible pixels after piecing together just four data sets. Because of recent technological advances, especially in laser technology, digital data acquisition, and computer storage, we were able to develop this laser radar system that is reasonably fast, compact, and relatively inexpensive. Current research and development efforts in eye-safe microlasers[17–19] and advanced scanning technology[20] will enable future scanning laser radar systems operating in an eye-safe mode to acquire similar 3-D data in a fraction of the time.

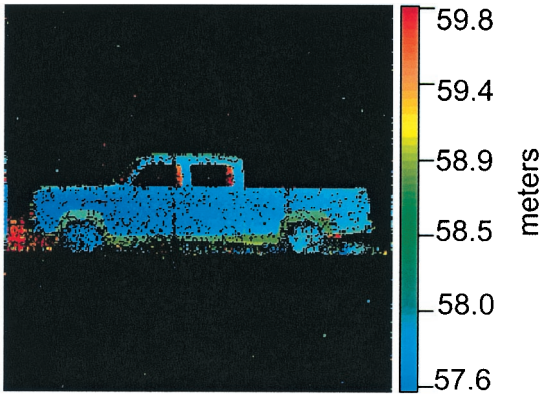

Fig. 17. Laser radar range data of truck behind heavy camouflage netting after four images are combined digitally.

References

1. E. R. Murray and J. E. van der Laan, "Remote measurement of ethylene using a CO_2 differential-absorption lidar," Appl. Opt. **17,** 814–817 (1978).
2. N. Menyuk, D. K. Killinger, and W. E. DeFeo, "Laser remote sensing of hydrazine, MMH, and UDMH using a differential-absorption CO_2 lidar," Appl. Opt. **21,** 2275–2286 (1982).
3. H. Ahlberg, S. Lundqvist, and B. Olsson, "CO_2 laser long-path measurements of diffuse leakages from a petrochemical plant," Appl. Opt. **24,** 3924–3928 (1985).
4. A. Ben-David, S. L. Emery, S. W. Gotoff, and F. M. D'Amico, "High pulse repetition frequency, multiple wavelength, pulsed CO_2 lidar system for atmospheric transmission and target reflectance measurements," Appl. Opt. **31,** 4224–4232 (1992).
5. C. B. Carlisle, J. E. van der Laan, L. W. Carr, P. Adam, and J.-P. Chiaroni, "CO_2 laser-based differential absorption lidar system for range-resolved and long-range detection of chemical vapor plumes," Appl. Opt. **34,** 6187–6200 (1995).
6. T. J. Kane, W. J. Kozlovsky, R. L. Byer, and C. E. Byvik, "Coherent laser radar at 1.06 μm using Nd:YAG lasers," Opt. Lett. **12,** 239–241 (1987).
7. A. N. Dills, G. Anderson, and R. J. Knise, "Holographic Raman/Rayleigh lidar for all-atmosphere thermal profiles," in *Laser Radar and Technology Applications VI,* G. W. Kamerman, ed., Proc. SPIE **4377,** 186–193 (2001).
8. J. A. Hutchinson, C. W. Trussell, T. H. Allik, S. J. Hamlin, J. C. McCarthy, and M. Jack, "Multifunction laser radar II," in *Laser Radar Technology and Applications V,* G. W. Kamerman, U. N. Singh, C. Werner, and V. V. Molebny, eds., Proc. SPIE **4035,** 248–253 (2000).
9. C. L. Smithpeter, R. O. Nellums, S. M. Lebien, and G. Studor, "A miniature, high-resolution laser radar operating at video rates," in *Laser Radar Technology and Applications V,* G. W. Kamerman, U. N. Singh, C. Werner, and V. V. Molebny, eds., Proc. SPIE **4035,** 279–286 (2000).
10. B. L. Stann, W. C. Ruff, and Z. G. Sztankay, "Intensity-modulated diode laser radar using frequency-modulation/continuous-wave ranging techniques," Opt. Eng. **35,** 3270–3278 (1996).
11. A. V. Jelalian, *Laser Radar Systems* (Artech House, Boston, Mass., 1991).
12. R. W. Byren, "Laser rangefinders," in *The Infrared and Electro-Optical Systems Handbook,* J. S. Accetta and D. L. Shumaker, eds. (Environmental Research Institute of Michigan, Ann Arbor, Mich. and SPIE, Bellingham, Wash. 1993).

13. T. N. Dreishuh, L. L. Gurdev, and D. V. Stoyanov, "Effect of pulse-shape uncertainty on the accuracy of deconvolved lidar profiles," J. Opt. Soc. Am. A **12,** 301–306 (1995).
14. Y. J. Park, W. S. Dho, and H. J. Kong, "Deconvolution of long-pulse lidar signals with matrix formulation," Appl. Opt. **36,** 5158–5161 (1997).
15. C. W. Trussell, "3D imaging for Army applications," in *Laser Radar and Technology Applications VI,* G. W. Kamerman, ed., Proc. SPIE **4377,** 126–131 (2001).
16. Q. Zheng, S. Der, and H. Mahmoud, "Model-based target recognition in pulsed ladar imagery," IEEE Trans. Image Process. **10,** 565–572 (2001).
17. J. E. Nettleton, B. W. Schilling, D. N. Barr, and J. S. Lei, "Monoblock laser for a low-cost, eyesafe, microlaser range finder," Appl. Opt. **39,** 2428–2432 (2000).
18. S. D. Setzler, P. A. Budni, and E. P. Chicklis, "A high energy Q-switched erbium at 1.62 microns," in *Advanced Solid-State Lasers*, C. Marshall, ed., Vol. 50 of OSA Trends in Optics and Photonics (Optical Society of America, Washington, D.C., 2001), pp. 309–311.
19. T. R. Schibli, T. Kremp, U. Morgner, F. X. Kärtner, R. Butendeich, J. Schwarz, H. Schweizer, F. Scholz, J. Hetzler, and M. Wegener, "Continuous-wave operation and Q-switched mode locking of Cr^{4+}:YAG microchip lasers," in *Advanced Solid-State Lasers,* C. Marshall, ed., Vol. 50 of OSA Trends in Optics and Photonics (Optical Society of America, Washington, D.C., 2001), pp. 343–345.
20. S. Masuda, S. Takahashi, T. Nose, S. Sato, and H. Ito, "Liquid-crystal microlens with a beam-steering function," Appl. Opt. **36,** 4772–4778 (1997).